Not for Publication
Presented Before the Division of Gas and Fuel Chemistry
American Chemical Society
Boston, Massachusetts, Meeting, April 5-10, 1959

X-RAY ANALYSIS OF ELECTRODE BINDER PITCHES AND THEIR COKES

Sidney S. Pollack and Leroy E. Alexander
Mellon Institute, Pittsburgh 13, Pa.

INTRODUCTION

The highly aromatic character of electrode binder pitches permits them to be studied by the same x-ray methods which have previously been applied to carbon blacks (1). The wide-angle x-ray scattering patterns are similar (see Figure 1) and show that both substances are built up of pseudocrystallites, or parallel-layer groups (to be referred to in this paper as crystallites), composed of graphite-like layers together with varying amounts of disorganized material. The quinoline soluble and insoluble fractions and the cokes of these pitches are also found to have a similar fine structure (Figure 1). All these materials, then, are composed principally of graphite-like layers, some of which are arranged turbostratically (2) in crystallites and some of which are unassociated. In the ensuing discussion we shall denote by D the fraction of disorganized material, by L_a and L_c the dimensions of the crystallites respectively parallel and normal to the constituent layers, by d_M the interlayer spacing, by M_e the effective number of layers in the crystallite, and by f_1, f_2, f_3, etc., the weight fractions of graphite-like layers respectively unassociated, associated in groups of two, associated in groups of three, etc.

The degree of physical heterogeneity of a specimen, whether it be due to the presence of particles, pores in solid matter, or discrete regions differing in density, is revealed by x-ray scattering at small angles. In favorable cases something can be learned about the shape and size distribution of the particles, or other entities, producing the scattering. In the present investigation we have employed the theory of x-ray scattering by dense systems which was developed by Kratky (13), Porod (16), and coworkers (9).

For clarity the wide-angle x-ray study will be presented first. This part of the paper will include a description of improvements in the experimental technique that have been adopted since the earlier report (1) and numerical results for fourteen samples, comprising six pitches and their 575° C. cokes and a beta resin and its 575° C. coke. The second part of the paper will deal with the small-angle scattering investigation of three pitches, their quinoline soluble and insoluble fractions, the 575° C. cokes of the pitches, and a beta resin. Finally some general conclusions will be drawn concerning the structure of electrode binder pitches and their cokes in the light of both the wide- and small-angle x-ray findings.

WIDE-ANGLE X-RAY ANALYSIS

Improvements in Experimental Procedure. Except for certain improvements to be described herewith, the counter diffractometric technique employed was the same as that described previously (1). As explained by Milberg (15), in studying specimens which are weakly absorbing to x-rays by the reflection technique, it is possible to make systematic errors in measuring intensities if the receiving slit is too narrow to permit the detector to "see" the entire irradiated volume of the sample. In the present study such errors were eliminated by removing the scatter slit of the Norelco goniometer. In Milberg's notation this means making a large with respect to A. Furthermore, the specimen dimensions were increased somewhat to permit intensities to be measured

over the angular range $2\theta = 12°$ to $144°$. The sample dimensions were 31 mm. long x 11 mm. wide x 8 mm. deep when used with a 1° divergence slit and 0.006-inch receiving slit.

CuKα radiation of rather high monochromatic character was obtained by using Ross balanced filters of nickel and cobalt (11,17). Satisfactory thicknesses were realized by varying them until both filters gave the same transmitted intensity at the wavelength of CuKβ, 1.392 A., while the Ni filter absorbed approximately 50% of CuKα, 1.542 A. The experimental counting rates were corrected for resolving time losses of the Geiger counter and for polarization in the usual way (1). Normalization of this corrected experimental curve (A in the notation of reference (1)) to electron units was accomplished by fitting it to the independent scattering curve (B) of carbon at the angle $(\sin\theta)/\lambda = 0.505$, a method suggested to one of the authors by P. B. Hirsch in a private communication. This method is justifiable on the basis of calculations by R. Diamond (4) of the x-ray scattering by discrete graphitic, or aromatic, layers of various sizes which demonstrate that the diffracted intensity is nearly independent of the layer dimension at this angle. As in the previous work the carbon scattering factors of McWeeny (14) were used; however, the values of the incoherent scattering computed by Keating and Vineyard (10) were employed rather than the earlier data tabulated by Compton and Allison.

In contrast to the previous investigation (1) the present study has made use of the (11) rather than (10) line in deducing the mean layer diameter $\underline{L}_a$ of the crystallites. There are two reasons for this change in choice of (hk) reflection. First, the reliability of the independent scattering curve of carbon is undoubtedly greater at the larger angle involved ($\underline{s} = 0.84$ rather than 0.49, where $\underline{s} = 2(\sin\theta)/\lambda$). Second, as noted by Diamond (4), the (hk) scattering function is less perturbed at this higher angle by the (00$\underline{\ell}$) interference function since the amplitudes of its maxima decay rapidly with increasing order, becoming negligible as a general rule for $\underline{\ell} > 4$. In this connection it may be mentioned that experience in this laboratory indicates that values of $\underline{L}_a$ derived from the (10) line tend to be larger than those derived from the (11) line, although this does not invariably hold.

INTERPRETATIVE PROCEDURE AND RESULTS

The several structural parameters, $\underline{D}$, $\underline{L}_a$, $\underline{L}_c$, $\underline{d}_M$, $\underline{M}_e$, and the fractions $\underline{f}_1$, $\underline{f}_2$, $\underline{f}_3$, etc., have been calculated from the experimental intensity curves in much the same way as was done in the last study. (1) As before, the (002) line profile has been converted to the symmetrical form $\underline{I}'$ by means of the proper choice of $\underline{D}$ in the equation

$$I' = \frac{s^2}{0.0606} \times \frac{I - D}{1 - D} . \qquad (1)$$

This choice of $\underline{D}$ can be made directly if equation (1) is first converted to the form

$$D = \frac{s_2^2 I_2 - s_1^2 I_1}{s_2^2 - s_1^2} , \qquad (2)$$

wherein $\underline{I}_1$ and $\underline{I}_2$ are the experimental intensities at two points $\underline{s}_1$ and $\underline{s}_2$ equidistant from the point of maximum intensity and close to the minima that lie on either side of the (002) maximum. For example, the angles $\underline{s}_1 = 0.16$ and $\underline{s}_2 = 0.40$ may be used if the maximum point falls very close to 0.28.

The $\underline{L}_a$ dimension of the crystallites has been computed in two ways (Table I): first, by using the Warren equation for the height of an (hk) profile as applied by Franklin (6) (see reference (1), equations (5) and (6)); second, from the width of the (11) profile at half-maximum intensity using the Scherrer crystallite size

formula with an appropriate value of the shape factor, $K = 1.84$, (12,19)

$$L_a = \frac{1.84\,\lambda}{w \cos\theta} . \qquad (3)$$

Both these methods of calculating L_a make the implicit assumption that any given specimen contains crystallites with a single uniform L_a dimension. Obviously this is not as realistic as a distribution of L_a values. Diamond (5) has recently described a least-squares method for selecting the most probable distribution of L_a's from the shape of an (hk) profile. Also the L_c dimension has been computed in two ways: first, through the use of the effective number of layers, M_e, which makes allowance for the distribution of M values; second, from the width of the (002) band at half-maximum intensity by means of the Scherrer crystallite size formula

$$L_c = \frac{0.9\,\lambda}{w \cos\theta} , \qquad (4)$$

in which the shape factor is set equal to 0.9. The second method does not take account of the distribution of M values.

The trial-and-error procedure described previously (1) was used to match the experimental and theoretical I' profile of the (002) band. This process leads to a picture of the distribution of M values characterizing each sample, which is to say, the weight fractions of graphite-like (aromatic) layers combined into crystallites composed of one layer (f_1), two layers (f_2), three layers (f_3), etc. Although this frequently leads to rather precise fitting of the (002) profile, it does not mean that the solution is unique. In fact, a study of the effect of controlled variations δf_1, δf_2, δf_3, etc., upon the quality of the fit obtained has shown that rather large deviations may be tolerated in f_1, f_2, and f_3 provided only that they are mutually complementary (f_2 increased at the expense of f_3 for example). This leads to the following estimate of probable deviations which apply to the various f's:

f_1	± 0.05
f_2, f_3	± 0.03
f_4, f_5, f_6	± 0.02
f_7, $\cdots$ f_{12}	± 0.01

These limits should be kept in mind in comparing the M distributions of the fourteen samples represented by histograms in Figure 2. These include six electrode binder pitches and their cokes and a beta resin and its coke. To emphasize the effect of coking at 575° C. on the association of layers, the coke histogram (broken lines) of each specimen has been superposed upon the histogram of the corresponding uncoked specimen (solid lines). It is evident that coking results in an increased degree of association of layers, the histograms tending to extend to higher M's with a decrease in the f's at lower M's. It is interesting to note, however, that in some cases coking increases the weight fraction of single layers, f_1, and in other cases decreases it.

Figure 3 compares the I' (002) profiles of pitch No. 3 and its coke. The greater asymmetry of the pitch profile is typical of all the specimens studied to varying degrees. It is probably the consequence of a considerable variation in the interlayer spacing, d_M. The nature of the skewness can be explained by crystallites with comparatively few layers having larger values of d_M than those with more layers. Semi-quantitative efforts to determine the upper and lower limits on d_M result in maximum values as large as 4.0 A. if the minimum value of 3.44 A. proposed by Franklin (7) for disordered layers is accepted. The presence of aliphatic material would also contribute to skewness of the type observed, and this would result in calculated D values which are too small. However, the aromatic content of the pitches studied is

so high as to eliminate this as a substantial source of error.

It is not possible to achieve a completely satisfactory matching of theoretical and experimental profiles for such skewed profiles on the basis of a single value of $\underline{d}_M$, as is done in the present scheme of analysis. At the same time the mathematical complexities arising from the use of a variable $\underline{d}_M$ parameter are so great as to exclude this approach in practice. It is well to bear in mind, then, that the $\underline{M}$ distributions deduced for the pitches are somewhat less reliable than those for the cokes, which produce more symmetrical $\underline{I}'$ (002) profiles.

Table I lists the $\underline{L}_a$ and $\underline{L}_c$ dimensions of the crystallites together with the parameters $\underline{D}$, $\underline{d}_M$, and $\underline{M}_e$, which were described earlier. The effective number of layers per crystallite is defined by

$$M_e = \sum_M f_M M , \tag{5}$$

and $\underline{L}_c$ is then given by

$$L_c = d_M M_e = d_M \sum_M f_M M . \tag{6}$$

In equation (6) $\underline{d}_M$ is computed from the $\underline{s}$ value corresponding to the point of maximum intensity of the $\underline{I}'$ (002) profile using the relation

$$d_M = 1/s_{max} . \tag{7}$$

It is to be emphasized that a single but different experimental value of $\underline{d}_M$ is derived for each specimen, but that a single constant value of 3.52 A. has been employed in the computation of all the theoretical (002) profiles in order to keep the mathematical labor within bounds.

In Table II values of the "shape factor" $\underline{L}_a/\underline{L}_c$ have been computed for the six pitches and their cokes as well as for the uncoked and coked beta resin. These ratios make use of $\underline{L}_a$ from the (11) peak width and $\underline{L}_c$ as derived from (002) profile matching, which are considered to be the most reliable values. From the two tables it will be seen that the layer dimension $\underline{L}_a$ falls in the range 12-16 A. for both the pitches and the cokes, while the crystallite "height" $\underline{L}_c$ lies in the range 12-14 A. for the pitches but 16-19 A. for their cokes. Hence the pitch crystallites have approximately equal dimensions $\underline{L}_a$ and $\underline{L}_c$ (average $\underline{L}_a/\underline{L}_c = 1.07$), whereas when coking occurs the crystallites grow more rapidly along $\underline{c}$ than $\underline{a}$ (for cokes the average $\underline{L}_a/\underline{L}_c = 0.77$).

From Table I it is seen that so-called "disorganized matter" constitutes from 30 to 50% of the mass of both the pitches and their cokes. This is appreciably higher than in carbon blacks where the usual limits are between 10 and 35%. It is also somewhat surprising that the fraction of disorganized matter in pitches is not appreciably larger than in their cokes. We may again note in this connection that the presence of aliphatics would tend to result in an underestimation of $\underline{D}$.

In order to understand what disorganized matter means we must remember that all x-ray interference effects, both crystalline reflections and amorphous halos, are the result of x-ray scattering by pairs of atoms separated by a frequently encountered vector distance or by systems of atoms arranged in a periodic fashion (lattices). On the other hand all interatomic vector distances of random, or very irregular, lengths result in continuous diffuse scatter which is part of the background scatter of the diffraction record. It is this continuous scatter, indistinguishable from the theoretical independent scatter of isolated atoms, which is interpreted by the present analytical method as being due to disorganized material. Therefore, disorganized matter consists only in part of fragmentary aggregates of carbon and other atoms. A

Table I. Crystallite Structure Parameters of Six Electrode Binder Pitches and a Beta Resin and Their 575° C. Cokes

(W-F = Warren-Franklin analysis)

	$\underline{D}$	$\underline{L_a}$ (A.) (W-F)	$\underline{L_a}$ (A.) (width)	$\underline{L_c}$ (A.) (distrib.)	$\underline{L_c}$ (A.) (width)	$\underline{d_M}$ (A.)	$\underline{M_e}$
Estimated Precision (probable deviation)	±0.05	±1.5	±1.5	±0.5	±0.5	±0.03	±0.20
1. Pitch	0.44	16.3	13.2	14.1	14.3	3.51	4.03
Coke	0.42	17.1	12.0	18.8	27.8	3.48	5.41
2. Pitch	0.39	14.5	15.3	12.7	13.9	3.52	3.60
Coke	0.36	14.2	13.1	17.8	26.4	3.52	5.05
3. Pitch	0.48	14.2	13.5	13.5	13.2	3.57	3.79
Coke	0.32	10.8	15.3	15.8	22.5	3.47	4.56
4. Pitch	0.44	15.6	12.1	12.4	12.9	3.52	3.51
Coke	0.51	20.0	12.4	17.3	22.5	3.50	4.95
5. Pitch	0.44	13.4	16.4	11.8	11.8	3.60	3.27
Coke	0.43	18.0	14.1	18.1	24.0	3.47	5.23
6. Pitch	0.46	10.4	12.4	12.6	13.2	3.52	3.59
Coke	0.45	12.0	13.3	16.4	27.5	3.50	4.69
7. Beta resin	0.52	23.8	13.9	12.0	12.5	3.55	3.39
Beta resin coked	0.38	17.6	14.8	19.1	18.0	3.55	5.39

Table II. Shapes of Crystallites

(L_a/L_c = ratio of diameter to height)

Sample No.		L_a/L_c of Pitches	L_a/L_c of Cokes (575° C.)
1		0.94	0.64
2		1.20	0.74
3		1.00	0.97
4		0.98	0.72
5		1.39	0.78
6		0.98	0.81
	Average	1.07	0.77
7	Beta Resin	1.16	0.78

considerable, if not major, part consists of other atoms irregularly located with respect to their nearer neighbors. Another way of saying this is that all departures of the atomic arrangement in the sample from ideality (ideal graphite layers associated in a random layer lattice), which is to say structural imperfections, will contribute to the diffuse background scatter and be recognized in part as disorganized matter. Thus the following will be interpreted, at least in part, as disorganized matter: foreign atoms (O, N, S, H, etc.), variations in the interlayer spacing from whatever causes, buckling of the layers due to possible non-aromatic character in certain regions, holes in the aromatic layers, and translational irregularity in the stacking of the layers one upon the other. J. R. Townsend (18) has made theoretical studies which show quantitatively that this kind of stacking disorder reduces the intensity of the (002) band and at the same time contributes to the diffuse background.

SMALL-ANGLE X-RAY ANALYSIS

Experimental Procedure. The x-ray scattering intensities at small angles were recorded manually using a General Electric XRD-5 diffraction apparatus equipped with a pair of identical 0.05° slit collimators (Type 4954BE) and argon proportional counter tube (Type A4952E). As in the wide-angle measurements, balanced nickel and cobalt filters were used to provide x-ray intensities of relatively high monochromatic character. Figure 4 is a schematic drawing of the apparatus with the receiving collimator (No. 2) set at the 0° 2θ position so as to receive the direct beam transmitted by collimator No. 1. The specimen is oriented with its surface normal to the direct beam. It turns through an angle $\Delta\theta$ about the spectrogoniometer axis when the receiving system turns through an angle $2\Delta\theta$, as is the usual arrangement in powder diffractometers. Although this causes the specimen to be inclined slightly when the small-angle scattering is being recorded, the x-ray absorption correction is not perceptibly changed because of the small angles involved. This means that an absorption correction need not be included in the interpretation of the intensity data. The slits 1a, 1b, 2a, and 2b are of equal dimensions, the width being about 0.04 mm. and the height being comparatively very large and determined by the separation of the Soller plates. These are sets of parallel plates with a spacing chosen so as to limit the vertical divergence to a tolerable amount.

The specimen powders were packed in a rectangular window 0.2 cm. thick by 0.4 cm. wide by 1.38 cm. long in a brass plate, no binders or adhesives being used. In terms of the specimen weight w, volume v, and known solid density d_s, the volume fraction of solid matter is then

$$c = \frac{\text{macro density}}{\text{solid density}} = \frac{w}{d_s v} .$$

The volume fraction of void space is, of course, $1 - c$. Counting rates were recorded point by point from $2\theta = 0.04°$ to a maximum angle beyond which the intensity was too low to measure accurately without prohibitively long counting times. This upper angular limit ranged from 0.3° for some pitches, quinoline soluble fractions, and the beta resin to 1.0° for all of the quinoline insoluble fractions. For each specimen the scattering curve was recorded (a) with Ni filter, (b) with Co filter, and then with specimen removed (c) with Ni filter, and (d) with Co filter. The difference of curves (c) and (d) gives a measure of the correction to be applied for parasitic scattering (scatter due to slits, air, and other extraneous sources). The correction curve is obtained by multiplying the directly measured curve by the absorption factor characterizing the particular specimen being examined, $\exp(-\mu t)$, where μ is the linear absorption coefficient of the sample and t is its thickness. The exponent μt can be directly obtained from the weight-to-area ratio (w/A) of the specimen by the following transformation:

$$\mu t = \frac{\mu}{d_s} \times \frac{d_s t A}{A} = \frac{\mu}{d_s} \times \frac{w}{A} . \qquad (8)$$

In this expression $(\mu/\underline{d}_s)$ is the mass absorption coefficient of the specimen for x-rays and $\underline{A}$ is the area of the face of the specimen normal to the beam (0.4 x 1.38 = 0.552 cm.^{2} for the specimen holder employed). The composition of each of the specimens was regarded as being 100% carbon, for which $\mu/\underline{d}_s$ was assigned the value measured by Chipman, (3) 4.15. Hence in the present study $\mu\underline{t} = 7.52\ \underline{w}$. The intensity curve to be analyzed was obtained from the several measured curves as follows:

$$I = (I_{Ni} - I_{Co})_S = (I_{Ni} - I_{Co})_{NS} \exp(-\mu t).$$

Here S = sample and NS = no sample.

Interpretative Procedure and Results. For a full explanation of the interpretative procedure the reader is referred to the paper by Kahovec et al. (9) Guinier and Fournet (8) have given a condensed account of the theory and requisite experimental conditions. The necessity for making corrections for finite slit height has been avoided by employing slits of large height-to-width ratio. The theory takes into account this experimental feature implicitly, (9,16) so that the formulas presented herewith require no modification for the "slit effect".

The first step in the analysis of the intensity curves is to compute the following quantities:

$$e = \int_0^\infty Ids . \qquad (9)$$

$$q = \int_0^\infty Isds . \qquad (10)$$

$$a = \lim_{s \longrightarrow \infty} (Is^3) . \qquad (11)$$

In these expressions $\underline{s} = (4\pi \sin\theta)/\lambda$, or $4\pi\theta/\lambda$ since θ is very small. It is seen that $\underline{e}$ is the integral scattered intensity over the entire range of appreciable intensity. Its value cannot be determined accurately in cases where $\underline{I}$ is still increasing rapidly at the lowest angle attainable. It can be shown theoretically that the scattering curve must in a completely general way approach asymptotically the line $\underline{s}^{-3}$ at higher angles, so that if the curve is multiplied by $\underline{s}^3$ a constant limiting value of $\underline{a}$ is reached. When this condition is experimentally realized, it becomes possible to determine the specific surface of the specimen. For some types of heterogeneity this asymptotic value is not reached at angles for which $\underline{I}$ is of detectable intensity, in which event the specific surface cannot be determined directly. A convenient way to apply this initial criterion is to plot intensity against $\underline{s}$ (or 2θ) on log-log paper and note whether a slope of approximately -3 is reached at the highest angles. This log-log plot also reveals something of the type of structure of the colloidal system. A flat mid-section means rod- or plate-like particles rather than a spherical or granular habit, a steeper slope as the primary beam is approached indicates clustering of particles into larger aggregates, while a decreasing slope as the primary beam is approached denotes the presence of a considerable proportion of particles of relatively small size. If the slope is uniformly close to -3 throughout the measurable range, the particles are regarded as rather uniform in size and approximately spherical in shape.

If an asymptotic slope of -3 is reached at the higher angles, the total surface area can be computed in terms of the volume fraction of solid from a and q as follows:

$$O = 4Vc\,(1 - c)\,a/q\,, \tag{12}$$

from which the surface in m.^{2} per cm.^{3} of solid sample is

$$O_r = \frac{O}{V_c} = 40{,}000\,(1 - c)\,\frac{a}{q}\,, \tag{13}$$

and the specific surface in m.^{2} per g. is

$$O_{sp} = \frac{40{,}000\,(1 - c)\,a}{d_s q}\,. \tag{14}$$

The theoretical expressions set forth by Porod, Kahovec, and associates also include three other useful quantities. The first is f, the structure number, defined by

$$f = ea/q^2\,. \tag{15}$$

This quantity is qualitatively a measure of the irregularity of the colloidal subdivision. In a dilute system of identical spheres f is about 1/2. Cluster formation, fluctuations in particle size, and deviations from spherical shape cause an increase in f, so that for granular structures in general it is close to unity. Still larger f's indicate pronounced departures from spherical shape.

The theory also yields two length parameters, $\overline{\ell}$ and ℓ_c. The first is the inhomogeneity length,

$$\overline{\ell} = 40{,}000/O_r\,. \tag{16}$$

If the colloidal system is imagined to be pierced by rays in all directions at random, the rays will be cut into different lengths by the disperse phase (particles in void or holes in solid). The numerical average of these lengths is $\overline{\ell}$. The second length parameter, ℓ_c, is known as the coherence length and is given by

$$\ell_c = 2e/q\,. \tag{17}$$

It is related to the size and shape of the particles as well as to their arrangement. In a dilute system of identical spheres ℓ_c is equal to 3/4 of the sphere diameter. Clustering of particles will cause an increase in the value of ℓ_c.

Table III gives results for three electrode binder pitches and their cokes, quinoline insoluble (Q.I.) fractions, and quinoline soluble (Q.S.) fractions, and for a beta resin. Figure 5 shows the plots of log I against log 2θ. Before attempting an interpretation of the numerical data in Table III it is best to see what can be learned from the curves. Perhaps the most obvious feature of the curves is their similarity in shape. With few exceptions they slope upwards at the lowest angles, an indication of either particle clustering or the presence of a substantial weight fraction of much larger particles. This is a conspicuous characteristic of all the specimens except the quinoline insoluble fractions, of which only one displays this feature. The slopes of all the curves tend to decrease continuously, although sometimes irregularly, with increasing angle. Hence there is no indication of pronounced departure from a spherical particulate habit. Finally, for most of the specimens the slopes

Table III. Small-Angle Scattering Results for Selected Samples

	Scattering Range (°2θ)	$\underline{e}$ (arbitrary units)	$\underline{f}$ (value directly computed)	$\underline{f}$ (value used in computing $\underline{\ell}$ and O_{sp})	$\underline{\ell}$ (A.)	$\overline{\ell}$ (A.)	O_{sp} ($m.^2/g.$)
Pitches							
No. 1	0.04-0.3	247	0.42		542		
No. 3	0.04-0.3	373	0.39		540		
No. 6	0.04-0.3	210	0.45		545		
Cokes							
No. 1	0.04-0.6	749	0.55	0.60	446	619	37.0
No. 3	0.04-0.7	1600	0.43	0.60	437	629	36.3
No. 6	0.04-0.6	1046	0.45	0.60	463	574	40.0
Q.I. Fractions							
No. 1	0.04-1.0	2939	0.38	0.60	423	623	39.0
No. 3	0.04-1.0	3832	0.54	0.54	384	698	34.7
No. 6	0.04-1.0	5333	0.59	0.59	362	577	42.0
Q.S. Fractions							
No. 1	0.04-0.3	446	0.34		548		
No. 3	0.04-0.3	230	0.43		541		
No. 6	0.04-0.4	706	0.42		527		
Beta Resin	0.04-0.3	786	0.49		518		

become considerably less than -3 at the largest angles, which means that in these instances the surface areas will have to be estimated by an indirect approach rather than determined directly in terms of the limiting value of $\underline{a} = \underline{I}\underline{s}^3$. Kahovec et al. suggest for such cases that a reasonable value be assigned to $\underline{f}$ and that a value of $\underline{a}$ be computed from it by means of equation (15). In Table III this method has been followed for cokes 1, 3, and 6 and Q.I. fraction 1, using an assigned $\underline{f}$ value of 0.60. The corresponding $\underline{\ell}$ and $\underline{O}_{sp}$ values are therefore to be regarded as estimates and less accurate than the values for Q.I. fractions 3 and 6.

The observations just made are in accord with the small values of $\underline{f}$ directly computed from the experimental intensities by means of equation (15). For Q.I. fractions 3 and 6 the limiting slope of the log $\underline{I}$ versus log $\underline{s}^3$ curve is close to -3, permitting dependable specific surface values to be calculated using equation (14). For the other samples the slopes become -3 at intermediate angles and yield the directly computed $\underline{f}$ values given in Table III, many of which are smaller than the theoretical minimum value of 0.50 to be expected for an ideal system of uniform spheres. These abnormally small values are not unexpected since a slope of -3 at large angles is not reached. A choice of $\underline{f} = 0.60$ seems reasonable as a basis for subsequent calculation of $\underline{a}$, $\underline{\ell}$, and $\underline{O}_{sp}$ since this is approximately the value observed for Q.I. fractions 3 and 6, which are believed to be reliable. The fact that all the directly computed $\underline{f}$'s are in the neighborhood of 0.5 emphasizes what has been already inferred from the curves, that the particle shape is not far from spherical.

It will be seen from Table III that the amount of small-angle scattering, $\underline{e}$, is largest for the Q.I. fractions, considerably less for the cokes, and very small for the pitches and Q.S. fractions. This shows that the Q.I. samples are most heterogeneous physically, the cokes less so, and the pitches and Q.S. samples relatively homogeneous. The weak small-angle scattering of the last two materials can be interpreted in two ways. First, it may mean that the samples are very largely solid continuums, without pores or particles, but that a small portion of each sample is either particulate or consists of solids with pores. Second, it may mean that the samples are entirely solid without pores or particles, but that the solid continuum consists of regions of differing density. The latter explanation seems more reasonable in the case of pitches and Q.S. fractions, but since the densities of the hypothetical constituent regions are not known, it is not worthwhile to compute specific surface values, which would necessarily rest on extremely arbitrary assumptions. Even if an effective "internal" surface could be computed in this way, it would have only a very ambiguous physical significance. In this connection it may be emphasized that small-angle scattering cannot differentiate between particles in void and the complementary case of pores in solid. Precisely complementary structures of these two kinds would give identical small-angle scattering patterns. Likewise, the specific surface would be the same in both cases and its determination unambiguous.

One of the two length parameters, the coherence length $\underline{\ell}_c$, is computed directly from the intensity integrals $\underline{e}$ and $\underline{q}$ (see equation (17)) and can be derived independently of the -3 slope criterion discussed above. Accordingly $\underline{\ell}_c$ has been calculated for all the specimens in Table III, whereas $\underline{\ell}$, the inhomogeneity length, and $\underline{O}_{sp}$, the specific surface, have been determined only for the cokes and Q.I. fractions. In deriving the specific surfaces, the values of $\underline{c}$ used have been those calculated from the following "solid" densities: 1.75 g./cm.^{3} for cokes and 1.65 g./cm.^{3} for Q.I. fractions.

Not only do the x-ray results indicate an approximately spherical habit for all the materials studied, but the length parameters $\underline{\ell}_c$ and $\underline{\ell}$ and the specific surfaces are surprisingly similar. This is striking in view of the probable difference in character of the heterogeneity in cokes and in Q.I. fractions. Thus one may be predominantly particulate whereas the other may be more reticular (pores in solid). Electron photomicrographs of the Q.I. fractions confirm the small-angle scattering results by showing most of the particles to be spherical, a considerable portion

being less than 1000 A. in diameter and the rest much larger on the average. Most of the cokes, however, are seen to consist of roughly equidimensional particles of otherwise irregular shape, many of them too large to produce small-angle scattering in the accessible angular range.

In the absence of supplementary information regarding the character of the heterogeneity in a substance that produces small-angle x-ray scatter, it is best to look upon $\mathcal{L}_c$ and $\mathcal{L}$ as giving the approximate linear dimensions of the structural entities responsible for the small-angle scatter instead of attempting a more concrete interpretation in terms of sphere or pore diameters. For all five substances studied these scattering entities are of nearly the same mean size, and in addition they are not far from spherical (at least equidimensional) in shape.

CONCLUSIONS

1. The fine structure of electrode binder pitches and their cokes resembles that of carbon blacks. Approximately two-thirds of the carbon is present as aromatic, or graphite-like layers, which for the most part are in turn aggregated into turbostratic crystallites.

2. Roughly one-third of the carbon and minor constituent elements are present as so-called disorganized material, a higher proportion than in carbon blacks.

3. The pitch and coke crystallites are approximately equidimensional with linear dimensions of 12-20 A. Coking of a pitch at 575° C. produces a somewhat greater increase in L_c than in L_a.

4. The interlayer spacing in pitch crystallites shows considerable variation, in contrast with those in cokes or carbon black, which are rather uniform.

5. A considerable portion, probably more than half, of the quinoline insoluble fractions examined is present in the form of roughly spherical particles with a mean diameter of the order of 500 A. The remainder is present as much larger particles the dimensions of which cannot be measured by small-angle x-ray scattering.

6. The small-angle scattering produced by pitches and their quinoline soluble fractions is weak, showing that they possess little if any particulate character.

7. 575° C. cokes of pitches and the quinoline insoluble fractions of pitches possess similar specific surfaces of the order of 40 $m.^2/g.$

ACKNOWLEDGMENTS

This work was done by the Chemical Physics Group at Mellon Institute and was supported by the Coal Chemicals Fellowship of the U. S. Steel Corporation. The electron microscope observations were made by Robert V. Rice.

REFERENCES

(1) Alexander, L. E., Sommer, E. C., J. Phys. Chem. 60, 1646 (1956).
(2) Biscoe, J., Warren, B. E., J. Appl. Phys. 13, 364 (1942).
(3) Chipman, D. R., J. Appl. Phys. 26, 1387 (1955).
(4) Diamond, R., Acta Cryst. 10, 359 (1957).
(5) Ibid., 11, 129 (1958).
(6) Franklin, R. E., Ibid., 3, 107 (1950).
(7) Ibid., 4, 253 (1951).
(8) Guinier, A., Fournet, G., "Small-Angle Scattering of X-Rays," pp. 78-81, 156-60, John Wiley, New York, 1955.
(9) Kahovec, L., Porod, G., Ruck, H., Kolloid Z. 133, 16 (1953).

(10) Keating, D. T., Vineyard, G. H., Acta Cryst. 9, 895 (1956).
(11) Kirkpatrick, P., Rev. Sci. Instr. 10, 186 (1939); 15, 223 (1944).
(12) Klug, H. P., Alexander, L. E., "X-Ray Diffraction Procedures for Polycrystalline and Amorphous Materials," pp. 516, 536, John Wiley, New York, 1954.
(13) Kratky, O., Naturwiss. 26, 94 (1938); 30, 542 (1942).
(14) McWeeny, R., Acta Cryst. 4, 513 (1951).
(15) Milberg, M. E., J. Appl. Phys. 29, 64 (1958).
(16) Porod, G., Kolloid Z. 124, 83 (1951); 125, 51 (1952).
(17) Ross, P. A., Phys. Rev. 28, 425 (1926).
(18) Townsend, J. R., Acta Cryst., in press.
(19) Warren, B. E., Phys. Rev. 59, 693 (1941).

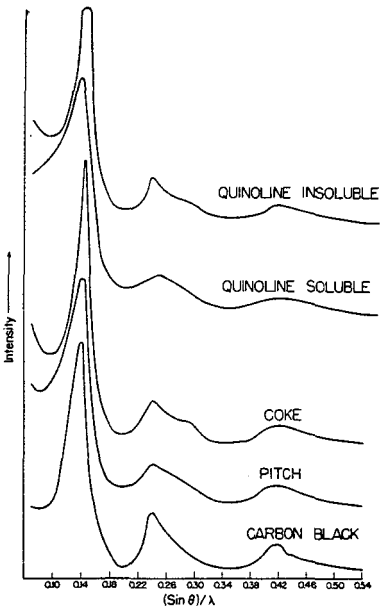

Figure 1. Comparison of the wide-angle x-ray diffraction patterns of an electrode binder pitch, its 575° C. coke, quinoline soluble and insoluble fractions of a pitch, and a typical carbon black

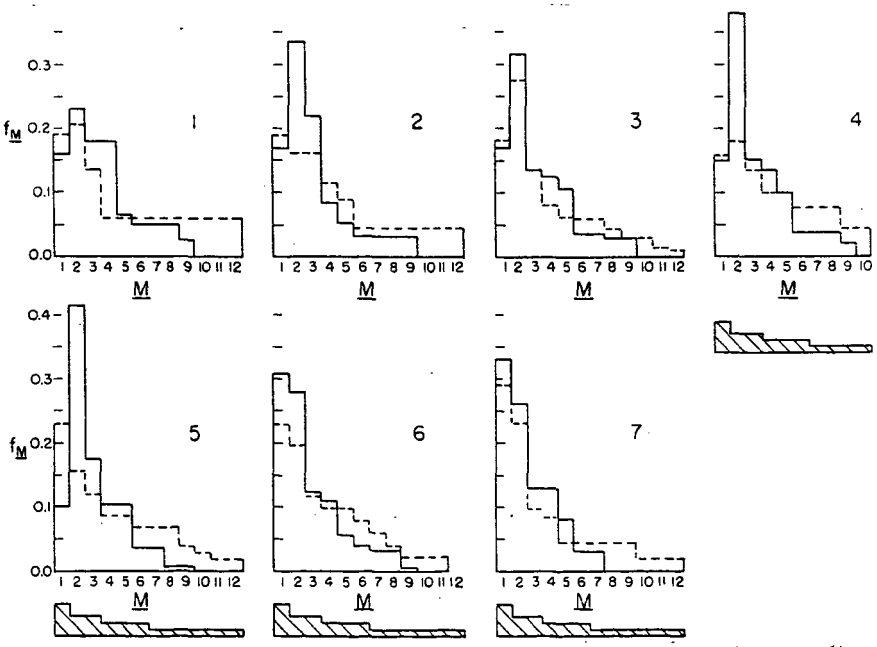

Figure 2. Histograms comparing the M distributions in six pitches (Nos. 1-6), a beta resin (No. 7), and their respective 575° C. cokes. Solid lines uncoked, broken lines coked. Estimated precision of f_M's indicated by hatched histograms.

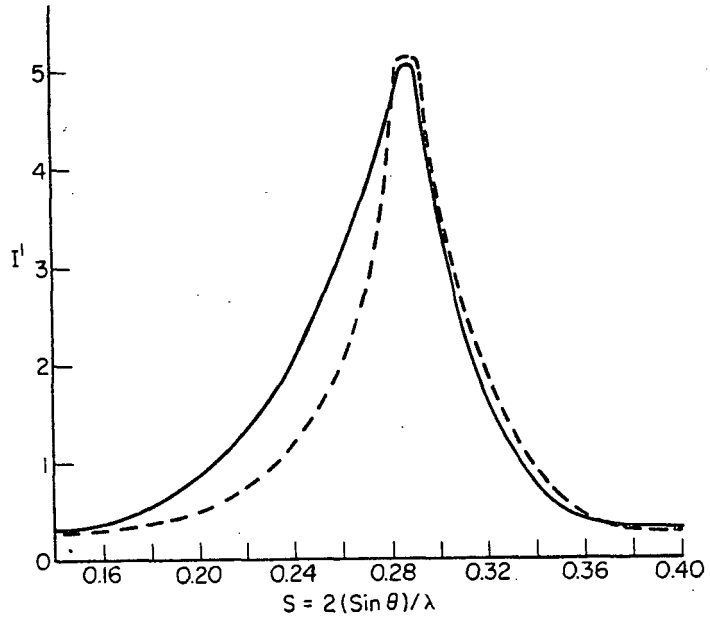

Figure 3. Comparative (002) profiles of pitch No. 3 (solid line) and its 575° C. coke (broken line).

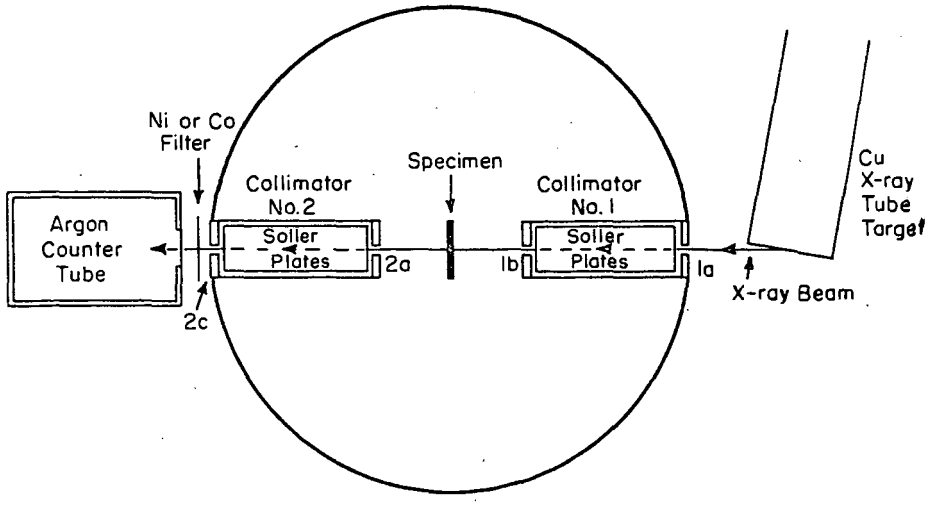

Figure 4. Schematic diagram of small-angle scattering apparatus.

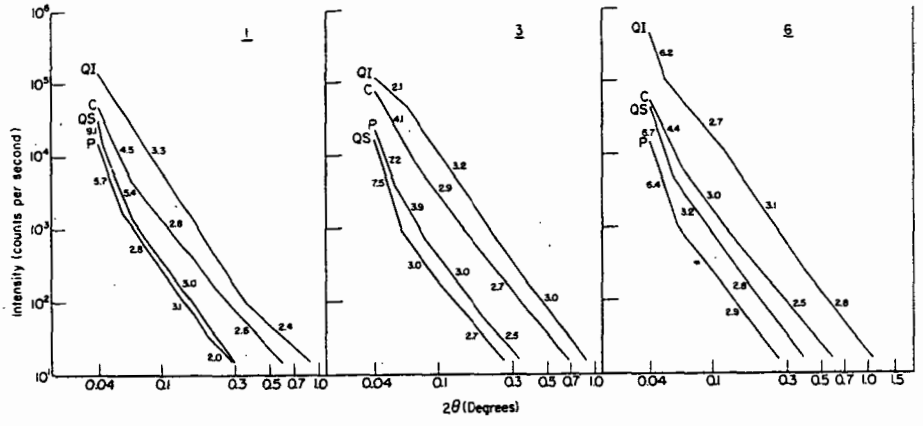

Figure 5. Plots of $\log_{10}I$ versus $\log_{10}2\theta$ for three electrode binder pitches (P), their 575° C. cokes (C), quinoline insoluble fractions (QI), and quinoline soluble fractions (QS). Numbers on curves indicate magnitudes of the negative slopes.